Atomic Structure of Ferredoxin-NADP$^+$ Reductase: Prototype for a Structurally Novel Flavoenzyme Family

P. ANDREW KARPLUS,* MARK J. DANIELS, JON R. HERRIOTT

The three-dimensional structure of spinach ferredoxin-NADP$^+$ reductase (NADP$^+$, nicotinamide adenine dinucleotide phosphate) has been determined by x-ray diffraction at 2.6 angstroms (Å) resolution and initially refined to an *R* factor of 0.226 at 2.2 Å resolution. The model includes the flavin-adenine dinucleotide (FAD) prosthetic group and the protein chain from residue 19 through the carboxyl terminus at residue 314 and is composed of two domains. The FAD binding domain (residues 19 to 161) has an antiparallel β barrel core and a single α helix for binding the pyrophosphate of FAD. The NADP binding domain (residues 162 to 314) has a central five-strand parallel β sheet and six surrounding helices. Binding of the competitive inhibitor 2′-phospho-AMP (AMP, adenosine monophosphate) places the NADP binding site at the carboxyl-terminal edge of the sheet in a manner similar to the nucleotide binding of the dehydrogenase family. The structures reveal the key residues that function in cofactor binding and the catalytic center. With these key residues as a guide, conclusive evidence is presented that the ferredoxin reductase structure is a prototype for the nicotinamide dinucleotide and FAD binding domains of the enzymes NADPH–cytochrome P450 reductase, NADPH-sulfite reductase, NADH–cytochrome b_5 reductase, and NADH-nitrate reductase. Thus this structure provides a structural framework for the NADH- or NADPH-dependent flavoenzyme parts of five distinct enzymes involved in photosynthesis, in the assimilation of inorganic nitrogen and sulfur, in fatty-acid oxidation, in the reduction of methemoglobin, and in the metabolism of many pesticides, drugs, and carcinogens.

IN PHOTOSYNTHESIS, LIGHT ENERGY, WHICH IS INITIALLY concentrated in a single excited electron in the photosynthetic reaction center, is partly used to create a proton gradient that can be converted to adenosine triphosphate (ATP) by the chloroplast adenosine triphosphatase (ATPase) and partly stored as reducing equivalents in NADPH through the action of ferredoxin-NADP$^+$ reductase (FNR, E.C. 1.18.1.2), the subject of this study (*1, 2*). For the production of NADPH, excited electrons from photosystem I reduce the one-electron–carrying iron-sulfur protein ferredoxin. Two ferredoxin molecules then successively pass on their electrons to the FAD prosthetic group of FNR, which becomes reduced first to the neutral flavin semiquinone and then to the fully reduced form before both electrons can be passed on to NADP$^+$ in the form of a hydride [Eq. 1 (*1, 3*)]

$$2 \text{ ferredoxin (reduced)} + \text{NADP}^+ + \text{H}^+ \rightarrow 2 \text{ ferredoxin (oxidized)} + \text{NADPH} \quad (1)$$

Since electrons are transferred from two molecules of an obligatory one-electron donor to a single molecule of a two-electron (hydride) acceptor, FNR is a member of the class of enzymes called dehydrogenases–electron transferases (*4*). The entry ports to all biological redox chains contain a flavoprotein dehydrogenase–electron transferase that catalyzes the transfer of electrons between nicotinamide, succinate, or fatty acid and the one-electron–carrying electron-transfer proteins. Amino acid sequence comparisons have shown that FNR may be related to the flavoenzymes cytochrome P450 reductase, cytochrome b_5 reductase, sulfite reductase, and nitrate reductase (*5–7*). We have undertaken crystallographic studies of FNR from spinach to determine the structural features of the protein that influence the electronic properties of the flavin and allow such versatility in catalysis.

The localization, regulation, enzymology, and structure-function relations of FNR have been comprehensively reviewed (*1*). The x-ray structure of spinach FNR at 3.7 Å resolution allowed a general description of the domain structure of the molecule, but a complete chain tracing was not possible (*8*). On the basis of the amino acid sequence, a partial model for the NADP-binding domain was built, but an interpretation of the FAD binding domain remained elusive (*9*). We have now extended the multiple isomorphous replacement analysis to a resolution of 2.6 Å and have carried out partial refinement of the model at 2.2 Å resolution. We present a description of the overall structure of the enzyme, identify key residues involved in function, and discuss familial relations of FNR.

Structure determination. FNR was purified from spinach chloroplast membranes and crystallized by the hanging drop method (*10*). Single crystals belonging to space group *C*2 (a = 90.7 Å, b = 57.7 Å, c = 68.1 Å, β = 100°), and apparently equivalent to those studied by Sheriff and Herriott (*8*), grew within a few weeks. The $UO_2(NO_3)_2$ and K_2 $Pt(CN)_4$ derivatives used in the low-resolution study (*8*) were selected for higher resolution work, and 2.2 Å resolution data sets for the native enzyme and these two derivatives were collected (*11*) (Table 1). Heavy-atom models obtained in the lower resolution work (*8*) were used to initiate

P. A. Karplus and M. J. Daniels are in the Department of Biochemistry, Molecular and Cell Biology, Cornell University, Ithaca, NY 14853. J. R. Herriott is in the Department of Biochemistry, University of Washington, Seattle, WA 98195.

*To whom correspondence should be addressed.

Table 1. X-ray data collection and phasing statistics. Phasing statistics given are the figure of merit for phasing the native data set and the phasing power (the ratio between the rms heavy-atom scattering amplitude and the lack of closure error) for each of the derivative data sets. The native and derivative data were collected with two multiwire area detectors (*11*). A single crystal was used for each data set and the data were reduced on site. The 2′-phospho-AMP data set was collected in four shells of equal reciprocal space volume on a Nicolet R3M diffractometer. Data were reduced by standard procedures (*44*); R_{sym} and R_{nat} are the R factors ($\Sigma|F_1 - F_2|/\Sigma F_2$) between Friedel pairs within a data set (number of pairs given in parentheses) and between a derivative and the native data sets. Factors to scale the derivative sets to the native data and to put all data on an absolute scale were calculated (*45*) and fixed during heavy-atom refinement. The relative temperature factors (ΔB) are given.

Data set	Data collection statistics					Phasing statistics versus resolution (Å)				
	Resolution (Å)	Unique reflections (No.; percentage of possible)	R_{sym}	R_{nat}	ΔB (Å^2)	∞–6	6–4	4–3	3–2.6	2.6–2.2
Native	2.2	15,980 (90)	0.049 (11,087)		0.0	0.85	0.75	0.68	0.58	0.51
Platinum	2.2	16,452 (93)	0.046 (10,950)	0.133	−0.2	2.2	2.0	1.7	1.7	1.3
Uranyl	2.2	15,650 (88)	0.077 (5,013)	0.192	1.9	1.4	1.4	1.1	1.0	0.8
2′-Phospho-AMP	3.0	7,065 (100)	0.092 (225)	0.137	0.8					

parameter refinement and phase determination (*12*). On the basis of the final statistics of the refinement (Table 1), and after comparison of electron density maps calculated at 2.6 or 2.2 Å resolution, 2.6 Å resolution was chosen as the cutoff for calculating electron density maps to be used for model building. The majority of the chain could be followed in this 2.6 Å map, and in particular the flavin and distinct strands of β sheet in the FAD binding domain could be located. However, large "ghost peaks" (*13*) were associated with the major heavy-atom positions and a few surface loops were not easily interpreted. The clarity of the map was improved by applying a density modification procedure to reduce systematic and random errors in the phases by flattening the peaks at the heavy-atom sites and in the solvent region (*14*).

The improved electron density map and the program FREIBAU (*15*) were used to build a model for the FAD prosthetic group and residues 21 to 314 of the protein chain. This model has been crystallographically refined against the data between 7 and 2.2 Å resolution from an R factor of 0.394 to 0.226 while maintaining reasonable geometry (*16*). During refinement, electron density was found for two extra residues at the amino terminus, so that the current model begins at residue 19. The loop from residues 236 to 243 has weak density and its conformation is not well determined. In Fig. 1 the quality of the current electron density distribution is illustrated.

Crystallographic location of the NADP binding site. The NADP binding site had been located at 3.7 Å resolution by difference Fourier analysis of crystals soaked with 100 mM NADPH (*8*). Quantitative analysis (*17*), however, indicated that the occupancy of binding was as low as 30 to 40 percent. To better define the binding site, we collected a 3 Å resolution data set from crystals soaked with 2′-phospho-AMP (Table 1). This fragment of NADPH acts as a competitive inhibitor with an inhibition constant K_i = 2 μM (*18*). The signal in the difference Fourier analysis was much stronger and the occupancy was estimated at 80 to 100 percent. Starting with the coordinates of the refined unliganded structure, seven residues (Ser^{204}, Pro^{205}, Arg^{235}, Lys^{244}, Tyr^{246}, Gln^{248}, and Leu^{274}) that had clearly moved during ligand binding were manually adjusted and coordinates for 2′-phospho-AMP were added. The model was refined against the data between 7 and 3 Å to an R factor of 0.196 (*16*).

FNR has two structural domains. The first 18 residues of FNR are not visible in the electron density map. We have verified by SDS–gel electrophoresis that dissolved crystals contain the intact enzyme, so we conclude that these residues are disordered. This result is consistent with observations that the amino terminus is susceptible to proteolytic nicking (*9, 19*), that this nicking does not affect in vitro enzymatic activity, and that the sequence of FNR from *Spirulina* begins at the equivalent of residue 23 of the spinach enzyme (*10, 20*).

An overview of the backbone structure of FNR shows its two-domain nature (Fig. 2A). The first domain, residues 19 through 161, binds the FAD prosthetic group, and the second domain, residues 162 through 314, contains the NADPH binding site. Each domain is a compact structure that provides for binding the bulk of its respective dinucleotide, although each dinucleotide also interacts with some residues from the other domain. Also, the domains have an extensive contact surface and may not be functionally separable. The interface between the two domains buries ~2800 Å^2 (1400 Å^2 per domain) (*21*). A single *cis*-proline occurs at residue 150.

FAD is bound to a β barrel structure. The core of the FAD

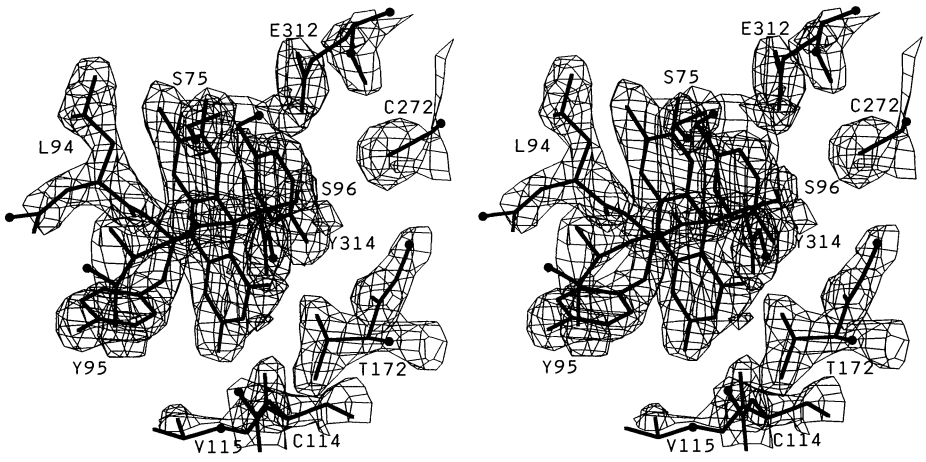

Fig. 1. Stereoview showing quality of the final $[2F_o - F_c]\alpha_{calc}$ electron density map and the environment of the enzyme bound flavin. The contour level for the density is at 20 percent of the maximum. Amino acid residues shown are labeled with the one-letter code (*46*). Density maxima which represent water molecules are apparent near the hydroxyl of Tyr^{314}, off of the carbonyl of Ser^{96}, and next to the carboxylate of Glu^{312}. The line of sight is nearly along the hydrogen bond from the peptide amide of residue 96 to the N5 atom of the flavin. Bumps due to the carbonyl groups and even a slight forking of the side-chain density for branched side chains (Leu^{94} and Thr^{172}) are clearly visible in the electron density.

domain is an antiparallel β barrel (Fig. 2, B and C). The use of this domain type for the binding of a flavin prosthetic group has not been seen in other flavoenzymes (*22*). As is common, the barrel is flattened and has distinct edges around which the neighboring strands are not as well hydrogen bonded. The top of the barrel is capped by the peptide segments from 98 to 108 and 65 to 75, while the bottom is covered by the helical segment from 131 to 137 (Fig. 2). In topological terms, it is a simple six-stranded, greek-key β barrel with a counterclockwise swirl (*23*). Other domains with this topology are found in trypsin and in pyruvate kinase. However, the FAD domain of FNR is distinguished from both of these structures (even as they are distinct from each other) by the spatial placement of the strands relative to each other and relative to the edge of the flattened barrel. In FNR the first two strands make a hydrogen-bonded ββ structure (Fig. 2), while in pyruvate kinase they are on opposite sides of the barrel and in trypsin the first three strands are adjacent (*23*).

The FAD prosthetic group is bound in an extended conformation with the flavin inserted into the protein at the domain boundary (Fig. 2, A and B). The polar environment around FAD is shown in Fig. 3. The ribose and adenine moieties of FAD are quite exposed and appear to make no direct hydrogen bonds to the protein, although some contact is made with the side chains of Leu^{118} and Tyr^{120}. The pyrophosphate group is stabilized by hydrogen bonds from the side chains of Arg^{93} and Ser^{133} and from all three of the peptide amides at the amino terminal end of the α helix from residues 131 to 137. Thus full advantage is made of the helix's ability to stabilize negative charges (*24*). The absence of a side chain at Gly^{130} is important to allow close approach of the helix to the pyrophosphate. Another prominent side chain involved in binding FAD is Tyr^{95}, which makes extensive van der Waals contact with the flavin and makes a hydrogen bond to the ribityl 3′-hydroxyl (Fig. 3).

The redox active part of FAD is the flavin, and the protein-flavin interactions must modulate its properties to allow control of one-electron and two-electron transfer. The flavin is bound external to the flattened β barrel at one of its edges (Fig. 2A). The flavin environment is shown in Figs. 1, 3, and 4. The Ser^{96} residue appears crucial as both its peptide amide and side chain interact with the catalytically competent N5 atom of the flavin. All hydrogen bonding between the protein and the flavin involves residues from the FAD-domain, which also serve to cover the back (*si*-face) of the flavin. The front (*re*-face) of the flavin points toward the NADP domain and is covered by the side chain of Tyr^{314}, which is stacked parallel to the flavin in such a way as to maximize π-orbital overlap. This interaction could explain the effective quenching of flavin fluorescence in FNR (*25*).

In accordance with chemical modification studies of FNR reconstituted with flavin analogs (*26*), only the edge of the dimethyl benzyl ring is well exposed to the solvent. The surrounding surface is made up by the side chains of Ser^{75}, Leu^{94}, and Glu^{312} (Fig. 1). By analogy with the electron carrier flavodoxin, single electron transfer probably occurs at this locus (*27*).

2′-Phospho-AMP binding identifies the functional NADP binding site. The NADP domain has a parallel five-stranded β sheet core and six surrounding helices (Fig. 2). The hydrogen-bonding pattern in the β sheet is regular and the sheet is large, with all strands having six or more residues. The twist of the sheet is about 5° per strand. The topology of the central β sheet (Fig. 2C) is equivalent to that seen for many dinucleotide binding proteins (*28*), but significant structural and functional differences exist (see below).

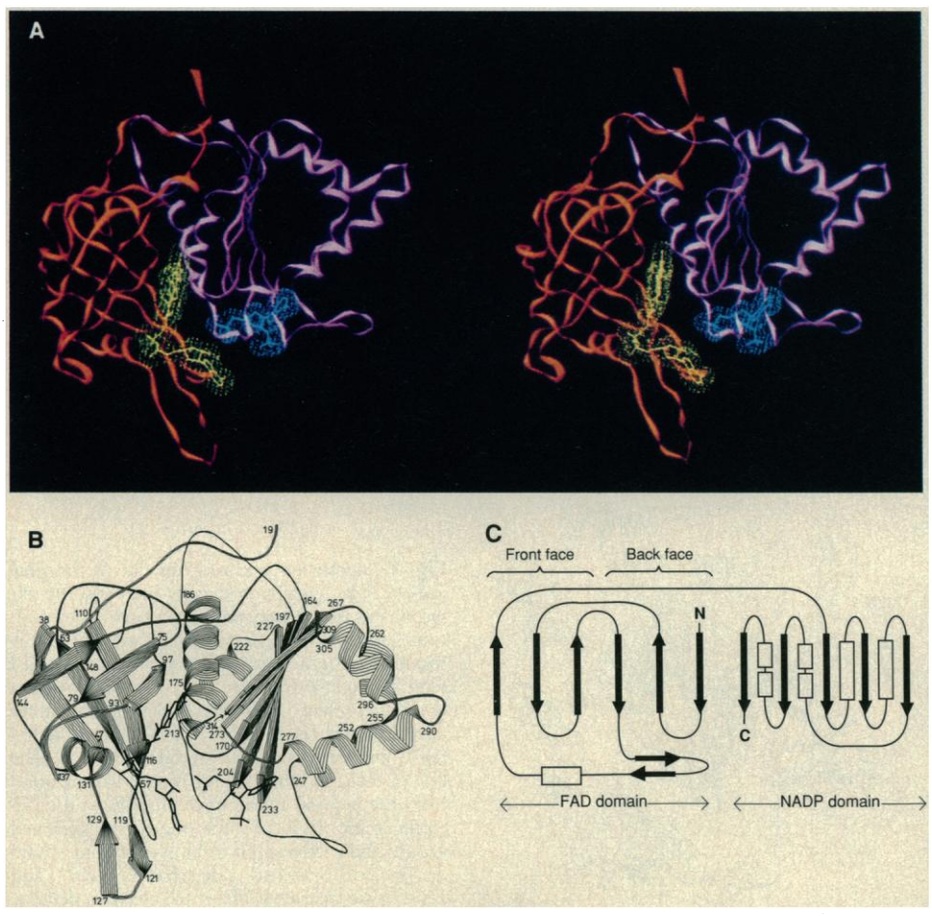

Fig. 2. Polypeptide chain folding and domain structure of FNR. (**A**) Stylized Cα backbone (*39*) of the whole protein: the FAD domain (red) and the NADP domain (magenta) are shown with models and van der Waals surfaces for FAD (yellow) and 2′-phospho-AMP (blue). The cleft where ferredoxin may bind faces the viewer. (**B**) Simplified ribbon diagram (*47*) of the secondary structural elements (*21*) of FNR, also showing the bound FAD and 2′-phospho-AMP. The view is similar to that in (A). (**C**) A two-dimensional topology diagram for FNR. Sheet strands and helices are represented by arrows and rectangles, respectively.

We have analyzed the binding of both NADPH (*8*) and 2′-phospho-AMP in FNR crystals. The 2′-phospho-AMP density is well formed with the two phosphates showing the highest electron density. 2′-Phospho-AMP binds at the carboxyl-terminal edge of the parallel sheets (Figs. 2 and 5), with the 5′-phosphate group approaching the glycine-rich loop (*9*) between the first strand of the sheet and the following helix. The side chain of Lys^{116} extends from the FAD domain to approach this phosphate. Probable hydrogen-bonding interactions with the protein are shown in Fig. 3B.

The ribose and adenine make hydrogen bonds with two main-chain carbonyls and the side chains of Thr^{170} and Gln^{248} (Fig. 3B). The 2′-phosphate forms four strong hydrogen bonds with the side-chain atoms of Ser^{234}, Arg^{235}, and Tyr^{246}. The amino group of Lys^{244} is 4 Å away and may interact weakly. Because the crystals are near pH = 4.5 (*8, 10*), the 2′-phosphate is probably protonated and only has a single negative charge. Under physiological conditions, it would be expected to carry a double negative charge and extra stabilization could be provided by a movement of Lys^{244}. These hydrogen bonds provide a structural explanation for the enzyme's discrimination against NAD^+, which lacks the 2′-phosphate group and has a K_m about 400-fold greater than that for $NADP^+$ (*2*). Both other structurally well-characterized $NADP^+$-dependent enzymes, dihydrofolate reductase (*29*) and glutathione reductase (*17, 30*), show a similar mechanism of discrimination.

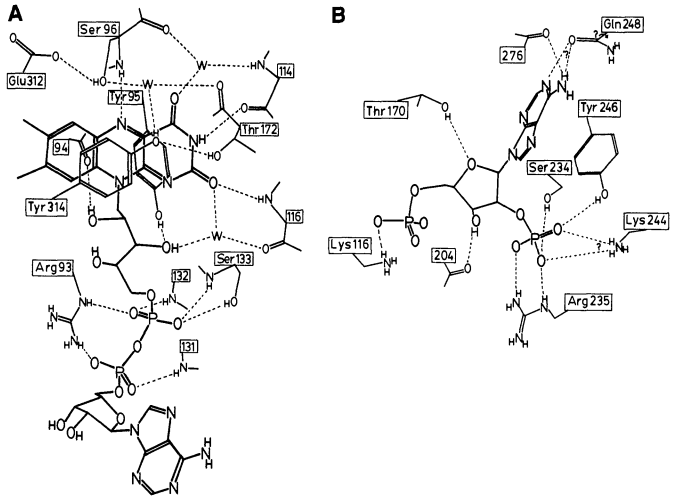

Fig. 3. Hydrogen bonding to and around enzyme-bound FAD and 2′-phospho-AMP. Probable hydrogen bonds between polar atoms less than 3.3 Å apart are shown as dashed lines. Residue numbers are given, and if side-chain atoms are involved, the amino acid type is also given. Hydrogen positions are not experimentally determined. (**A**) The FAD environment. Water molecules visible in the electron density (see Fig. 1) are shown as W. The side-chain hydroxyl of Ser^{96} is 3.4 Å from the flavin N5 atom and in position to receive a hydrogen bond from a reduced flavin. (**B**) The 2′-phospho-AMP environment. The interactions involving Lys^{244} and Gln^{248} are noted with a question mark because both separations are close to 4 Å and the orientation of the Gln^{248} amide is ambiguous. Both side chains, however, move toward the ligand during binding so a favorable polar interaction is probable.

Only minor conformational changes of the protein occur upon 2′-phospho-AMP binding, with nearly all of the hydrogen-bonding side chains moving toward the ligand. Also, the side chains of Leu^{274} (see Fig. 4) and Tyr^{246} move toward the adenine to make contact, and Pro^{205} is displaced by van der Waals contacts with the incoming ribose.

The difference electron density for bound NADPH is weak and not well formed (*8, 31*). It overlaps with the 2′-phospho-AMP binding site but is generally further from the enzyme surface. The highest density peaks, which were assigned to the pyrophosphate and the 2′-phosphate of NADPH (*8, 31*), correspond to the position of the adenine ring and the adenine ribose of 2′-phospho-AMP, respectively. The specific pocket occupied by the 2′-phosphate group of 2′-phospho-AMP is empty. The level of binding is much lower than would be expected based on a K_m of 1 μM under assay conditions (*18*) and must be due to either the buffer conditions in the crystal—high salt and low pH—or physical constraints on the structure caused by the molecular packing in the crystal.

Comparison of the mode of binding of 2′-phospho-AMP with the results of solution experiments and sequence comparisons (see below) provides support that its binding mode rather than that observed for NADPH is functionally relevant. Chemical modification experiments have implicated Lys^{116}, Lys^{244}, one of lysines 188, 193, 213, 218, 220, or 222, an arginine, carboxylate, and a histidine in NADPH binding (*1, 32*). The model shows that Lys^{116}, Lys^{244}, and Arg^{235} are directly involved in binding the 5′- and 2′-phosphates (Fig. 3B). No histidines or carboxylates, with the possible exception of the carboxyl terminus (Fig. 4), are directly involved, and none of the six lysines between residue 178 and 228 is near the observed binding site. These results can be explained, however, if the above groups were involved in a conformational change that

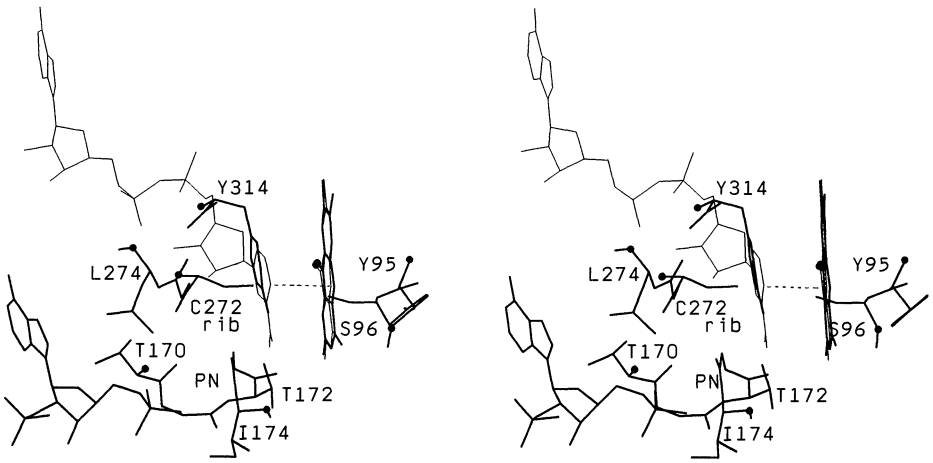

Fig. 4. The proposed binding site for the nicotinamide mononucleotide moiety of NADP. The FNR structure with 2′-phospho-AMP bound (bold lines) is compared with the flavin and NADH from glutathione reductase (thin lines) (*30*) after the two flavins have been superimposed (*48*). Places where the chain has been cut are marked by dots. The nicotinamide C4 atom and flavin N5 atom, between which hydride transfer takes place, are connected by a dashed line. We propose that in FNR the nicotinamide may also stack on the flavin in a similar way, but because the dinucleotide approaches from below instead of above, the nicotinamide carboxamide group would point up, overlapping the benzyl ring of the flavin. The proposed path from the 5′-phosphate of 2′-phospho-AMP to the nicotinamide is open in FNR and would place the second phosphate of the pyrophosphate at the position marked "PN" (in position to hydrogen bond to the backbone amide and possibly the side chain of Thr^{172}) and the ribose in the region marked "rib." To allow this binding, the side chain of Tyr^{314} would have to move out of the nicotinamide pocket, reminiscent of the movement of Tyr^{197} in glutathione reductase (*17*). As Tyr^{314} is at the enzyme surface, such a motion is feasible.

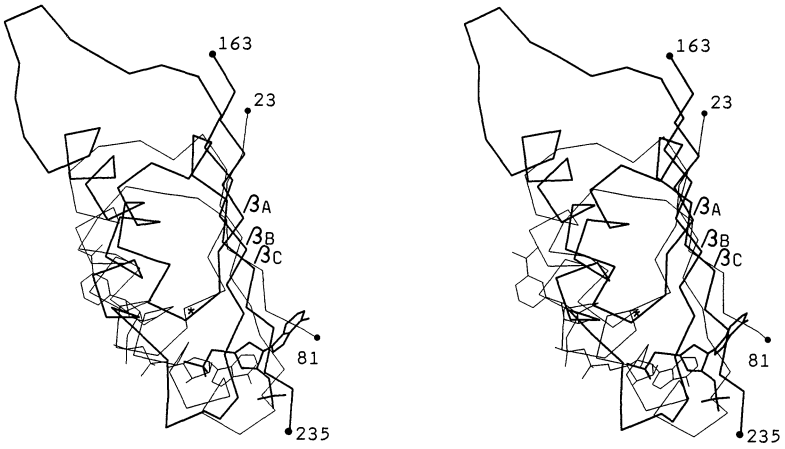

Fig. 5. Comparison of the nucleotide binding fold of FNR with that of lactate dehydrogenase. The bound nucleotide structure and the Cα backbone for the subdomain containing the first three strands of β sheet (marked β_A, β_B, and β_C) are shown for lactate dehydrogenase from pig heart (*35*) (thin lines) and FNR (thick lines). Chain breaks are marked with dots, and the end residues are labeled. The Cα positions of 20 equivalent hydrogen-bonding residues of the β sheet were used to calculate the best superposition (rms deviation = 1.1 Å) (*48*). The position of a conserved glycine that terminates strand β_A in both proteins is marked with an asterisk.

could occur when a complete molecule of NADPH binds properly.

How does the nicotinamide bind? Crystallographic studies of glutathione reductase have shown that hydride transfer occurs through a stacked nicotinamide-flavin interaction that places the nicotinamide C4 atom opposite the flavin N5 atom (*17, 30*). The structure of FNR is also compatible with such an interaction. When the flavins of the two enzymes are superimposed, the nicotinamide from glutathione reductase closely matches the position of the side chain of Tyr^{314} (Fig. 4), suggesting that this tyrosine may fill the nicotinamide binding pocket to maintain the enzyme structure and protect the flavin in the absence of NADP. The superposition also shows that the 5′-phosphate of 2′-phospho-AMP is at an appropriate distance (12 Å) from the proposed nicotinamide binding site and that the path from the 5′-phosphate to this site is not hindered (Fig. 4). Because the cofactor approaches from below in FNR (Fig. 4), the nicotinamide would have to be flipped in order to maintain an anti conformation and the opposite side of the nicotinamide would face the flavin. This result is in agreement with the stereospecificities of the enzymes: FNR is specific for transfer of the A-hydrogen, and glutathione reductase is specific for the B-hydrogen (*33*). In this hypothetical complex, the sulfhydryl of Cys^{272} is only 4 Å away from the C4 atom of the nicotinamide and thus may be functionally important (*34*).

Relation to known dinucleotide binding folds. To determine how the NADP domain of FNR relates to the commonly observed dinucleotide binding fold (*28*), we compared FNR to lactate dehydrogenase (*35*), which contains the prototypical dinucleotide binding fold. The sheets and the domains as a whole overlap well (as they must for any two parallel sheets of the same topology), but the substrate binding site in FNR is shifted about 5 Å to the right (Fig. 5), which allows the 2′-phosphate (or 2′-hydroxyl for NADH) to interact with residues at the end of β_C rather than β_B as in the typical dinucleotide binding fold. The loop between β_A and the following helix does still appear to be involved in binding of the pyrophosphate (Figs. 4 and 5), but makes a much tighter turn in FNR (Fig. 5). There is an apparent similarity in the sequence of the pyrophosphate binding loop in FNR, Gly-Thr-Gly-Xaa-Xaa-Pro (see Fig. 6; Xaa is an amino acid), with that of the canonical dinucleotide binding protein, Gly-Xaa-Gly-Xaa-Xaa-Gly, but the φ,χ angles of the first two conserved glycines in FNR are (53°, −122°) and (−65°, −5°), while the conformations for the canonical loop cluster around (100°, 120°) and (−120°, −160°) (*28*). These differences convince us that despite topological and functional similarities, a divergent evolutionary relation between this structure and the canonical dinucleotide binding domain cannot be assumed.

Ferredoxin recognition. In addition to FAD and NADPH, FNR must bind ferredoxin specifically. Chemical modification and cross-linking studies have indicated that Lys^{85} or Lys^{88} of FNR is near to a glutamic acid at residue 92, 93, or 94 of ferredoxin and that in addition, residues 26 to 30 and 65 to 70 of ferredoxin are important for binding (*36*). Lys^{85} and Lys^{88} of FNR are part of a surface loop ~20 Å from the exposed dimethylbenzyl portion of flavin. In this region the surface of FNR is extended and rather flat and is made up of residues 80 to 93 and the atoms of FAD itself (Fig. 2A). There is also electron density for a phosphate or sulfate ion bound to the side chains of His^{89}, Lys^{90}, and Arg^{93} (*37*).

Since the crystal structure of a plant-type ferredoxin from *Spirulina* is known (*38*), we have carried out preliminary modeling studies to show that the above data can be reconciled with the known structures of FNR and ferredoxin. We used computer graphics (*39*) to dock ferredoxin onto FNR by placing the iron-sulfur cluster of ferredoxin near the exposed portion of the flavin to

Ferredoxin-NADP$^+$ reductase	93	130	167	234	271	311	Reference
Spinach	...RLYSIAS...	GVCS...	MLGTGTGIAPF...	SREQTNEKGE**K**MYIQ...	MCG...	VEVY	*(9)*
Spirulina maxima	...RLYSIAS...	GVCS...	MMATGTGIAPF...	SREQQNPEGG**K**MYIQ...	ICG...	VETY	*(20)*
NADPH-cytochrome P450 reductase	453	487	529	595	627	672	
Human	...RYYSIAS...	GKMS...	MVGPGTGVAPF...	SREQ----SH**K**VYVQ...	VCG...	LDVWS	*(42)*
Yeast	...RYYSISS...	GVTT...	MIGPGTGVAPF...	SRLP---NTK**K**VYVQ...	VCG...	EDVWS	*(51)*
Bacillus megaterium	...RYYSISS...	GIAS...	MVGPGTGVAPF...	SRMP---NQP**K**TYVQ..	ICG...	KDVWAG	*(52)*
NADPH-sulfite reductase	386	419	457	519	551	596	
Escherichia coli	...RLYSIAS...	GGAS...	MIGPGTGIAPF...	SRDQ----KE**K**IYVQ...	VCG...	RDVY	*(7)*
NADH-cytochrome b_5 reductase	91	124	176	239	272	297	
Human	...RPYTPIS...	GKMS...	MIAGGTGITPM...	DRAP----EAWDYGQ...	MCG...	CFVF	*(53)*
NADH-nitrate reductase	712	745	781	854	888	914	
Arabidopsis thaliana	...RAYTPSS...	GLMS...	MLAGGTGITPV...	ESAK----EGWAYST...	ACG...	FLIF	*(6)*
Absolutely conserved	* *	*	*	*** *	*	**	

Fig. 6. Conservation of functional residues in the FNR family (*46*). Shown are six peptide segments from spinach FNR, containing 14 residues (in bold) for which the side chain is involved in the binding of either FAD or NADP. The equivalent segments from representative homologs are aligned (= designates a gap). The first entry for each enzyme type gives the residue numbers for the first amino acid in each segment. (The last residue shown is carboxyl-terminal residue in each case.) Each of the compared segments on its own is too short to indicate a homologous relation, but because the segments all appear in the same order along the chain and at similar spacings, the alignment as a whole becomes significant. When separate database searches were carried out with profiles (*49*) for the segments beginning at residues 93 and 167, and the scores from the two searches were multiplied together, the known family members gave the top scores and no new family members were found. The same concept of using well-conserved segments separated by variable gaps has been more fully developed by Barton and Sternberg to develop a filter which distinguishes all globin from non-globin sequences (*50*).

account for electron transfer, and Glu^{95} of ferredoxin (equivalent to Glu^{93} of spinach ferredoxin) next to Lys^{85} of FNR, while avoiding steric overlap of the molecules. In this orientation, ferredoxin fills the cleft between the two domains of FNR (Fig. 2A), as was predicted from the rotational correlation time of the complex (*32*), and is located close to the NADP binding site so that they may be interacting but non-overlapping as was suggested by solution studies (*1, 3*). No evidence is yet available to help locate recognition sites for other proteins that bind to FNR in vivo, or to address the structural mechanisms behind the observed allotopic modulation of FNR activity (*1*).

The ferredoxin reductase family. Sequence similarity exists between FNR and NADPH–cytochrome P450 reductase and, to a lesser degree, between FNR and NADH–cytochrome b_5 reductase (*5*). Recently, sequences for NADH-nitrate reductase (*6*) and NADPH-sulfite reductase (*7*) were shown to be fairly similar to cytochrome b_5 reductase and to cytochrome P450 reductase, respectively. Although these enzymes have striking functional similarities, for the more distantly related pairs, the sequence similarities are low, making sequence alignment difficult and the assumption of structural homology uncertain. With the three-dimensional structure of FNR now available, we can evaluate these relations based on the conservation of residues whose side chains are involved in the function of the enzyme. (The amino acid residues for which the main chain atoms are involved in function need not be as well conserved.)

Most of the residues with side chains involved in FAD and NADP binding are concentrated in six peptide segments (Fig. 6) and are well conserved among these enzymes. The only notable exceptions are Ser^{234}, Arg^{235}, and Lys^{244}, which function in the binding of the 2′-phosphate of NADP and hence vary for the two NADH-dependent enzymes. In particular, Ser^{234} changes to an acidic residue which, by analogy with NADH- and NADPH-dependent enzymes in the glutathione reductase family (*40*), could hydrogen bond to the ribose 2′-hydroxyl. This result argues for relatedness and provides further support for the functional relevance of the 2′-phospho-AMP binding mode.

Additional evidence that these enzymes form a family comes from considering key residues identified in the related enzymes. For instance, in cytochrome b_5 reductase, a Tyr residue (which we would now identify as Tyr^{93}) is known to interact with FAD, and a mutation of $Ser^{127} \rightarrow$ Pro disturbs enzyme function to cause methemoglobinemia (*41*). Likewise, in cytochrome P450 reductase, Cys^{471} (equivalent to Cys^{114} of FNR; see Fig. 1) was implicated in FAD binding, and Cys^{565} (equivalent to Val^{204} of FNR; see Fig. 3B) was implicated in NADP binding (*42*). Thus the dinucleotide binding domains of these proteins can be modeled based on the structure of FNR presented here. Glutathione reductase is, however, not a member of this family and structural and functional interpretations based on this comparison were misleading (*5*).

As more protein sequences are determined, additional members are likely to be added to this family. It is already clear, however, that the FNR family does not include all NADH- or NADPH-dependent dehydrogenase–electron transferases. The sequences of adrenodoxin reductase, long thought to be analogous to FNR, and rubredoxin reductase rule out the presence of an FNR-like fold and are consistent with the presence of more typical nucleotide binding domains (*43*).

REFERENCES AND NOTES

1. N. J. Carrillo and R. H. Vallejos, in *Topics in Photosynthesis*, J. Barber, Ed. (Elsevier, Amsterdam, 1987), vol. 8, pp. 527–560; R. Pschorn, W. Ruhle, A. Wild, *Photosynth. Res.* **17**, 217 (1988).
2. M. Shin and D. I. Arnon, *J. Biol. Chem.* **240**, 1405 (1965).
3. C. J. Batie and H. Kamin, *ibid.* **259**, 11976 (1984).
4. V. Massey and P. Hemmerich, *Biochem. Soc. Trans.* **8**, 246 (1980); P. Hemmerich, *Adv. Chem. Ser.* **162**, 312 (1977).
5. T. D. Porter and C. B. Kasper, *Biochemistry* **25**, 1682 (1986).
6. N. M. Crawford, M. Smith, D. Bellissimo, R. W. Davis, *Proc. Natl. Acad. Sci. U.S.A.* **85**, 5006 (1988).
7. J. Ostrowski *et al.*, *J. Biol. Chem.* **264**, 15796 (1989).
8. S. Sheriff and J. R. Herriott, *J. Mol. Biol.* **145**, 441 (1981).
9. P. A. Karplus, K. A. Walsh, J. R. Herriott, *Biochemistry* **23**, 6576 (1984); Y. Yao, K. Wada, Y. Takahashi, S. Katoh, H. Matsubara, *J. Biochem.* **98**, 1079 (1985).
10. E. C. Apley, R. Wagner, S. Engelbrecht, *Anal. Biochem.* **150**, 145 (1985). The protein was eluted from the DEAE-cellulose column by a linear gradient from 0 to 250 mM NaCl and the fractions containing FNR were directly applied to the procion-red affinity column. The shallower gradient on the DEAE column allowed better separation of FNR from the F_1-ATPase peak. The hydroxylapatite column was also eluted with a shallower gradient from 10 to 300 mM potassium phosphate. The purified protein ran as a single 36-kD band on SDS–gel electrophoresis and had a protein-to-flavin spectral ratio (absorbance at 276 nm versus 456 nm) of ~6.5. The reductase was stored at 3.4 mg/ml in 1 mM potassium phosphate, pH = 7.4, at −20°C. Crystallization was carried out by the hanging drop method at 4°C with a reservoir of 200 mM McIlvaines isocitrate-phosphate buffer, pH = 5.05, containing 1.4 to 1.5 M ammonium sulfate. The drop was formed by mixing 5 μl of the reservoir with 5 μl of the purified reductase solution. Crystals were stored in 0.1 M sodium acetate, pH = 4.5, with 55 percent saturated ammonium sulfate.
11. S. E. Sobottka, R. J. Chandross, G. G. Corrick, R. H. Kretsinger, R. G. Rains, *J. Appl. Crystallogr.* **23**, 199 (1990).
12. R. E. Dickerson, M. L. Kopka, J. C. Varnum, J. E. Weinzierl, *Acta Crystallogr.* **23**, 511 (1967). The isomorphous and anomalous differences of reflections with $F/\sigma(F) \geq 1$ were used to refine the heavy-atom coordinates and either the temperature factors or occupancies first at 3 Å, then at 2.6 Å, and finally at 2.2 Å resolution. Cross-phased difference Fourier maps were used to edit the heavy-atom sites, and the refinement process was carried to completion. That the anomalous signal was well measured and contributed favorably to the phase determination is indicated, in that the signs of the observed and calculated anomalous signal agreed for 82 and 73 percent of the reflections of the platinum and uranyl derivatives, respectively.
13. T. L. Blundell and L. N. Johnson, *Protein Crystallography* (Academic Press, London, 1976).
14. B. C. Wang, *Methods Enzymol.* **115**, 90 (1985); A. G. W. Leslie, *Acta Crystallogr.* **A43**, 134 (1987). A radius of 9 Å was used for determining the envelope and, so that the large electron density peaks at the heavy-atom sites would not influence the envelope, all points within 3.5 Å of heavy-atom sites were set to a density of zero before the envelope determination. Three 16-cycle passes of tethered refinement were made with values of 10, 25, and 40 percent for the bulk solvent content of the crystal (the true value is estimated to be 43 percent). During density modification the average absolute phase change was 30° (12° at low resolution to 40° at high resolution) and the average figure of merit rose to be near 0.9, independent of resolution.
15. The model was built at the Cornell Biotechnology Computer Facility with a Hewlett-Packard 9000/835 Turbo SRX workstation equipped with a Crystaleyes stereoviewing system (Stereo Graphics Corp., San Rafael, CA). FREIBAU was developed by P. A. Karplus and ported for use on a Hewlett-Packard workstation by G. Dykes, P. A. Karplus, and T. O'Conner.
16. D. E. Tronrud, L. F. TenEyck, B. W. Matthews, *Acta Crystallogr.* **A43**, 489 (1987). Restrained refinement of the coordinates and individual atomic temperature factors was carried out by the TNT program suite. Temperature factors were assigned to the initial coordinate set by the method of Fox and Karplus (unpublished results). During 25 cycles of coordinate refinement with data between 7 Å and 2.6 Å resolution, the R factor dropped from 0.368 to 0.231 ($R = \Sigma|F_o - F_c|/\Sigma F_o$, where F_o and F_c are the observed and calculated structure factors, respectively). After manual rebuilding, 20 further cycles of coordinate refinement and 11 cycles of temperature factor refinement yielded an R factor of 0.205. The resolution was then extended to 2.2 Å and 21 cycles of coordinate and 3 cycles of temperature factor refinement dropped the R factor from 0.245 to 0.217. After minor manual adjustments were made, the model was refined for five further cycles under tight geometric restraints to bring the final bond length and bond angle root-mean-square (rms) deviations to 0.024 Å and 3.0°, respectively. The 2′-phospho-AMP liganded structure underwent 24 cycles of coordinate refinement. Final bond length and bond angle deviations are 0.033 Å and 2.8°, respectively. No bound solvent molecules have been included in the models.
17. E. F. Pai, P. A. Karplus, G. E. Schulz, *Biochemistry* **27**, 4465 (1988).
18. C. J. Batie and H. Kamin, *J. Biol. Chem.* **261**, 11214 (1986).
19. M. Shin *et al.*, *Arch. Biochem. Biophys.* **279**, 97 (1990).
20. Y. Yao, T. Tamura, K. Wada, H. Matsubara, K. Kodo, *J. Biochem.* **95**, 1513 (1984).
21. W. Kabsch and C. Sander, *Biopolymers* **22**, 2577 (1983). Surface areas and secondary structure were calculated by the program DSSPNOV.
22. H. A. Schreuder, J. M. van der Laan, W. G. J. Hol, J. Drenth, *J. Mol. Biol.* **199**, 637 (1988); J.-J. P. Kim and J. Wu, *Proc. Natl. Acad. Sci. U.S.A.* **85**, 6677 (1988); W. W. Smith, R. M. Burnett, G. D. Darling, M. L. Ludwig, *J. Mol. Biol.* **117**, 195 (1977); Y. Lindqvist and C.-I. Branden, *J. Biol. Chem.* **264**, 3624 (1989); Z.-X. Xia and F. S. Mathews, *J. Mol. Biol.* **212**, 837 (1990); P. A. Karplus and G. E. Schulz, *ibid.* **195**, 701 (1987).
23. J. S. Richardson, *Adv. Protein Chem.* **34**, 167 (1981).
24. W. G. J. Hol, P. T. van Duijnen, H. J. C. Berendsen, *Nature* **273**, 443 (1978); W. G. J. Hol, *Prog. Biophys. Mol. Biol.* **45**, 149 (1985).
25. M. Shin, *Biochim. Biophys. Acta* **292**, 13 (1973).

26. G. Zanetti, V. Massey, B. Curti, *Eur. J. Biochem.* **132**, 201 (1983).
27. S. G. Mayhew and M. L. Ludwig, *Enzymes* **12**, 57 (1975); V. Favaudon and J.-M. Lhoste, *Biochemistry* **14**, 4731 (1975).
28. M. G. Rossmann, D. Moras, K. W. Olsen, *Nature* **250**, 194 (1974); M. G. Rossmann, A. Liljas, C.-I. Branden, L. J. Banaszak, *Enzymes* **11**, 61 (1975); R. K. Wierenga, M. C. H. DeMaeyer, W. G. J. Hol, *Biochemistry* **24**, 1346 (1985).
29. D. J. Filman, J. T. Bolin, D. A. Matthews, J. Kraut, *J. Biol. Chem.* **257**, 13663 (1982).
30. P. A. Karplus and G. E. Schulz, *J. Mol. Biol.* **210**, 163 (1989).
31. P. A. Karplus and J. R. Herriott, in *Flavins and Flavoproteins*, V. Massey and C. H. Williams, Jr., Eds. (Elsevier/North-Holland, New York, 1982), pp. 28–31. Figure 2 of this paper shows electron density for enzyme-bound NADPH.
32. D. Cidaria, P. A. Biondi, G. Zanetti, S. Ronchi, *Eur. J. Biochem.* **146**, 295 (1985); R. L. Chan, N. Carrillo, R. H. Vallejos, *Arch. Biochim. Biophys.* **240**, 172 (1985); E. C. Apley and R. Wagner, *Biochim. Biophys. Acta* **936**, 269 (1988).
33. G. Krakow, R. N. Ammeraal, B. Vennesland, *J. Biol. Chem.* **240**, 1820 (1965); B. K. Stern and B. Vennesland, *ibid.* **235**, 209 (1960).
34. D. J. Davis and A. San Pietro, *Arch. Biochem. Biophys.* **184**, 572 (1977).
35. U. M. Grau, W. E. Trommer, M. G. Rossmann, *J. Mol. Biol.* **151**, 289 (1981).
36. G. Zanetti *et al.*, *Biochemistry* **27**, 3753 (1988); B. J. Vieira, K. K. Colvert, D. J. Davis, *Biochim. Biophys. Acta* **851**, 109 (1986).
37. G. L. Ulrich and J. L. Markley, paper presented at 9th International Conference on Magnetic Resonance in Biological Sciences, Bendor, France, 1980. Actually two phosphate or sulfate ions appear to be bound in the crystal, one near His^{90} and one near Arg^{235} where the 2′-phosphate of 2′-phospho-AMP binds.
38. K. Fukuyama *et al.*, *Nature* **286**, 522 (1980); T. Tsukihara *et al.*, *Biosystems* **15**, 243 (1982).
39. D. Schomburg and J. Reichelt, *J. Mol. Graph.* **6**, 161 (1988).
40. N. S. Scrutton, A. Berry, R. N. Perham, *Nature* **343**, 38 (1990); D. W. Rice, G. E. Schulz, J. R. Guest, *J. Mol. Biol.* **174**, 483 (1984).
41. P. Strittmatter, *J. Biol. Chem.* **236**, 2329 (1961); Y. Kobayashi, Y. Fukumaki, T. Yubisui, J. Inoue, Y. Sakaki, *Blood* **75**, 1408 (1990).
42. M. Haniu, T. Iyanagi, P. Miller, T. D. Lee, J. E. Shively, *Biochemistry* **25**, 7906 (1986); M. Haniu, M. E. McManus, D. J. Birkett, T. D. Lee, J. E. Shively, *ibid.* **28**, 8639 (1989).
43. I. Hanukoglu and T. Gutfinger, *Eur. J. Biochem.* **180**, 479 (1989); G. Eggink, H. Engel, G. Vriend, P. Terpstra, B. Witholt, *J. Mol. Biol.* **212**, 135 (1990).
44. R. Thieme, E. F. Pai, R. H. Schirmer, G. E. Schulz, *J. Mol. Biol.* **152**, 763 (1981).
45. A. K. Singh and S. Ramaseshan, *Acta Crystallogr.* **21**, 279 (1966); A. J. C. Wilson, *ibid.* **2**, 318 (1949).
46. Abbreviations for the amino acid residues are A, Ala; C, Cys; D, Asp; E, Glu; F, Phe; G, Gly; H, His; I, Ile; K, Lys; L, Leu; M, Met; N, Asn; P, Pro; Q, Gln; R, Arg; S, Ser; T, Thr; V, Val; W, Trp; and Y, Tyr.
47. J. P. Priestle, *J. Appl. Crystallogr.* **21**, 572 (1988).
48. W. Kabsch, *Acta Crystallogr.* **A32**, 922 (1976); _____, *ibid.* **A34**, 827 (1978).
49. M. Gribskov, R. Luthy, D. Eisenberg, *Methods Enzymol.* **183**, 146 (1990).
50. G. J. Barton and M. J. E. Sternberg, *J. Mol. Biol.* **212**, 389 (1990).
51. Y. Yabusaki, H. Murakami, H. Ohkawa, *J. Biochem.* **103**, 1004 (1988).
53. T. Yubisui *et al.*, *ibid.* **96**, 579 (1984); S. Tomatsu *et al.*, *Gene* **80**, 353 (1989).
54. The complete refined coordinate sets for unliganded FNR, and FNR with 2′-phospho-AMP bound will be deposited in the Brookhaven Protein Data Bank.
We thank A. Jagendorf and B. Howlett for advice and for the use of laboratory facilities for the enzyme purification and S. Jacques for technical assistance. We also thank R. Kretsinger and R. Chandross for assistance in carrying out data collection and reduction at the MAXD Biotechnology Resource. The Hewlett-Packard workstations used for molecular graphics were generously donated by Hewlett-Packard Corporation. Supported by grants from the NSF (PCM 81-09700) and from the Cornell Biotechnology Program which is sponsored by the New York State Science and Technology Foundation, a consortium of industries, the U.S. Army Research Office, and the National Science Foundation.

27 June 1990; accepted 28 September 1990

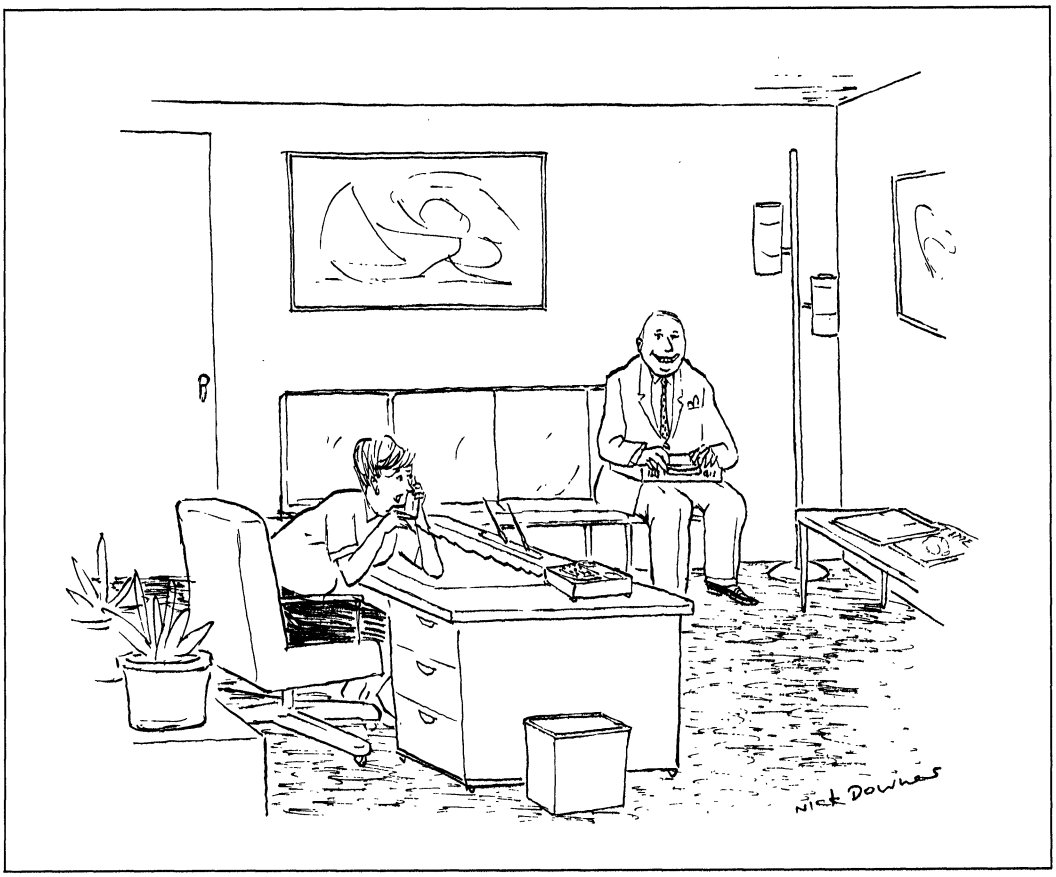

" I've managed to discourage the medical-supply salesmen, Doctor, but there's a leech farmer out here I just can't shake."